Image Fusion with Local Spectral Consistency and Dynamic Gradient Sparsity

Chen Chen[1], Yeqing Li[1], Wei Liu[2] and Junzhou Huang[1*]
[1]University of Texas at Arlington
[2]IBM T.J. Watson Research Center

Abstract

In this paper, we propose a novel method for image fusion from a high resolution panchromatic image and a low resolution multispectral image at the same geographical location. Different from previous methods, we do not make any assumption about the upsampled multispectral image, but only assume that the fused image after downsampling should be close to the original multispectral image. This is a severely ill-posed problem and a dynamic gradient sparsity penalty is thus proposed for regularization. Incorporating the intra- correlations of different bands, this penalty can effectively exploit the prior information (e.g. sharp boundaries) from the panchromatic image. A new convex optimization algorithm is proposed to efficiently solve this problem. Extensive experiments on four multispectral datasets demonstrate that the proposed method significantly outperforms the state-of-the-arts in terms of both spatial and spectral qualities.

1. Introduction

Multispectral (MS) images are widely used in many fields of remote sensing such as environmental monitoring, agriculture, mineral exploration etc. However, the design of MS sensors with high resolution is confined by infrastructure limits in onboard storage and bandwidth transmission [20]. In contrast, panchromatic (Pan) gray-scaled images with high spatial resolution can be obtained more conveniently because they are composed of much reduced numbers of pixels. The combinations of Pan images with high spatial resolution and MS images with high spectral resolution can be acquired simultaneously from most existing satellites. Therefore, we expect to obtain images in both high spatial resolution and high spectral resolution via image fusion (also called pan-sharpening).

Image fusion is a typical inverse problem and generally difficult to solve. A number of conventional methods use projection and substitution, which include principal component analysis (PCA) [6], intensity hue saturation (IHS) [11], wavelet [25] and their combinations. These methods work in the following scheme: upsampling, forward transform, intensity matching, component substitution and reverse transform [2]. Other methods such as Brovey [10], assume the Pan image is a linear combination of all bands of the fused image. A detailed survey of existing methods can be found in [2]. While these previous methods provided some good visual results, they are very likely to suffer from spectral distortion since their strong assumptions are not realistic in remote sensing physics [20].

In order to overcome the issue caused by spectral distortion, a suite of variational approaches have emerged recently [3][18][9]. Each method formulates an energy function based on somewhat weak assumptions, and minimizing such a function leads to the optimum. The first variational method P+XS [3] is based on the linear combination assumption in Brovey [10] and also assumes the upsampled MS image is the fusion result after blurring. As an accurate blur kernel is difficult to pre-estimate, AVWP [18] replaces this term with a spectral ratio constraint to preserve spectral information. It also forces the fused image to be close to the wavelet fused image [25]. Another variational model is engaged in estimating the fused image and the blurring model parameters iteratively [9]. Promising results have been achieved in these variational methods, especially they can reduce spectral distortion. However, due to the lack of an effective model to preserve spatial information, visible artifacts may appear on the fusion results.

In this paper, we propose a new variational model for image fusion to bridge this gap. Motivated by the geographical relationship between the fused image and Pan image, a dynamic gradient sparsity property is discovered, defined and then exploited to improve spatial quality. In addition, we assume the fused image after downsampling should be close the MS image, which is formulated as a least squares fitting term to keep spectral information. The combined model does not violate remote sensing physics. This is a key difference compared with previous methods. Moreover, our method incorporates the inherent correlation of different bands, which has not been considered before. To optimize

*Corresponding author. Email: jzhuang@uta.edu.

1063-6919/14 $31.00 © 2014 IEEE
DOI 10.1109/CVPR.2014.347

our entire energy function, a new algorithm is proposed in the fast iterative shrinkage-thresholding algorithm (FISTA) [4] framework, with a very fast convergence rate. Extensive experimental results demonstrate our method can significantly reduce spectral distortion while preserving sharp objects boundaries in the fused images.

2. Proposed Method

2.1. Notations

Scalers are denoted by lowercase letters. Bold letters denote matrices. Specially, $\mathbf{P} \in \mathbb{R}^{m \times n}$ denotes the Pan image and $\mathbf{M} \in \mathbb{R}^{\frac{m}{c} \times \frac{n}{c} \times s}$ denotes the low resolution MS image. c is a constant. For example $c = 4$ when the resolution of Pan image is 0.6m and that of MS image is 2.4m in Quickbird acquisition. The image to be fused is denoted by $\mathbf{X} \in \mathbb{R}^{m \times n \times s}$. $||\cdot||_F$ denotes the Frobenius norm. For simpleness, $\mathbf{X}_{i,j,d}$ denotes the element in i-th row, j-th column and d-th band in $\mathbf{X}$. And $\mathbf{X}_d$ denotes the whole d-th band, which is therefore a matrix.

2.2. Local Spectral Consistency

All the previous methods [3][18][9] use the upsampled MS image as prior knowledge to preserve spectral information. However, the upsampled MS image is often blurred and not accurate. Therefore, we only assume the fused image after downsampling is close to the original MS image. Least squares fitting is used to model this relationship:

$$E_1 = \frac{1}{2}||\psi\mathbf{X} - \mathbf{M}||_F^2, \tag{1}$$

where ψ denotes a downsampling operator. Local spectral information is forced to be consistent with each MS pixel. Similar as in previous works, the input images are assumed to be geometrically registered during preprocessing. As the remotely sensed images have geographical coordinates, the image registration is relatively easier.

Minimizing E_1 would be a severely ill-posed problem, due to the very low undersampling rate (e.g. 1/16 when $c = 4$). Without strong prior information, $\mathbf{X}$ is almost impossible to be estimated accurately. This may be the reason that all previous methods do not use this energy function.

2.3. Dynamic Gradient Sparsity

Fortunately, the Pan image provides such prior information. Due to the strong geographical correlation with the fused image $\mathbf{X}$, the Pan image has already provided us with clear boundary information of land objects. Many researchers attempt to build this relationship mathematically. From recent reviews [2][20], however, no model exists that can effectively characterize this relationship.

As remotely sensed images are often piece-wise smooth, their gradients tend to be sparse and the non-zeros corresponds to the boundaries. In addition, the positions of such boundaries should be the same as those on the Pan image. It demonstrates that the sparsity property is not fixed but dynamic according to a reference image. This property has not been studied in sparsity theories yet. We call the data with such a property a dynamic gradient sparse signal/image.

Definition: *Let $x \in \mathbb{R}^N$ and $r \in \mathbb{R}^N$ denote the signal and the reference signal. Ω_x and Ω_r denote the support sets*[1] *of their gradients, respectively. The set of dynamic gradient sparse signals is defined as:*
$\mathcal{S}_x = \{x \in \mathbb{R}^N : |\Omega_x| = K, \Omega_x = \Omega_r, \text{ with } K << N\}$.

Using similar logic, it can be extended to multi-channel/spectral signals and images. In previous methods P+XS [3] and AVWP [18], the ℓ_2 norm regularization is used to exploit the gradient prior information, which does not induce sparseness and tends to over-smooth the image by penalizing large values. In Fang's variational approach (FVP) [9], the first term is derived from the linear combination assumption in P+XS; it does not promote sparsity for each band. Different from previous work, dynamic gradient sparsity is encouraged in our method. Beside the prior information that previous methods attempt to use, we also notice the intra- correlations across different bands as they are the representations of the same land objects. Therefore, the gradients of different bands should be group sparse. It is widely known that the ℓ_1 norm encourages sparsity and the $\ell_{2,1}$ norm encourages group sparsity [24]. Thus we propose a new energy function to encourage dynamic gradient sparsity and group sparsity simultaneously:

$$E_2 = ||\nabla\mathbf{X} - \nabla D(\mathbf{P})||_{2,1} \tag{2}$$

$$= \sum_i \sum_j \sqrt{\sum_d \sum_q (\nabla_q \mathbf{X}_{i,j,d} - \nabla_q \mathbf{P}_{i,j})^2}, \tag{3}$$

where $q = 1, 2$ and $D(\mathbf{P})$ means duplicating $\mathbf{P}$ to s bands. ∇_1 and ∇_2 denote the forward finite difference operators on the first and second coordinates, respectively. Interestingly, when there is no reference image, i.e. $\mathbf{P} = \mathbf{0}$, the result is identical to that of vectorial total variation (VTV) minimization [5, 12, 7].

To demonstrate why E_2 encourages dynamic gradient sparsity, we show a simple example on a 1D multi-channel signal in Figure 1. We could observe that, if the solution has a different support set from the reference, the total sparsity of the gradients will be increased. Cases (a)-(d) have group sparsity number 8, 4, 4, 2 respectively. Therefore, (a)-(c) will be penalized because they are not the sparsest solution in our method.

Combining the two energy functions, the image fusion problem can be formulated as:

$$\min_{\mathbf{X}} \{E(\mathbf{X}) = E_1 + \lambda E_2 = \frac{1}{2}||\psi\mathbf{X} - \mathbf{M}||_F^2 + \lambda||\nabla\mathbf{X} - \nabla D(\mathbf{P})||_{2,1}\}, \tag{4}$$

[1] Here we mean the indices of the non-zero components.

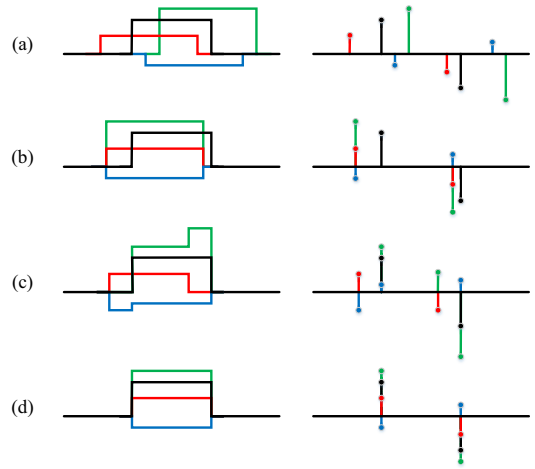

Figure 1. Illustration of possible solutions for different gradient based penalties. The black denotes a reference signal. RGB color lines denotes the solutions of different models. Left: 1D signals. Right: the corresponding gradients. (a) A possible solution of TV: the gradients of RGB channels are sparse but may not be correlated. (b) A possible solution of VTV: the gradients of R, G, B channels are group sparse, but may not be correlated to the reference signal. (c) A possible solution of FVP [9]: it does not encourage sparseness for each channel individually. (d) A possible solution of dynamic gradient sparsity regularization: the gradients can only be group sparse following the reference.

where λ is a positive parameter.

Comparing our method with existing methods [3][18][9], the first benefit of our method comes from the local spectral constraint. It does not rely on the upsampled MS image and linear-combination assumption. Therefore, only accurate spectral information is kept. It can be further applied to image fusion from different sources or different time acquisitions. Second, the proposed dynamic gradient sparsity only forces the support sets to be the same, while the sign of the gradients as well as the magnitudes of the signal are not required to be the same. These properties make it invariant under contrast inversion [20] and not sensitive to illumination conditions. Last but not least, only our method can jointly fuse multiple bands simultaneously, which provides robustness to noise [15][13]. These advantages exist in our method uniquely.

2.4. Algorithm

It is obviously that problem (4) is convex and has a global optimal solution. The first term is smooth while the second term is non-smooth. This motivates us to solve the problem in the FISTA framework [4, 14]. It has been proven that FISTA can achieve the optimal convergence rate for first order methods. That is, $E(\mathbf{X}^k) - E(\mathbf{X}^*) \sim \mathcal{O}(1/k^2)$, where $\mathbf{X}^*$ is the optimal solution and k is the iteration counter. We summarize the proposed algorithm for pan-sharpening in Algorithm 1.

Here ψ^T denotes the inverse operator of ψ. L is the Lipschitz constant for $\psi^T(\psi\mathbf{X} - \mathbf{M})$, which can be set as 1 in this problem. We could observe that the solution is updated based on both $\mathbf{X}^k$ and $\mathbf{X}^{k-1}$, while the Bregman method that used in previous methods [3][9] updates $\mathbf{X}$ only based on $\mathbf{X}^k$. This is a reason why our method converges faster. For the second step, $L = 1$ and

$$\mathbf{X}^k = \arg\min_{\mathbf{X}} \{\frac{1}{2}\|\mathbf{X} - \mathbf{Y}\|_F^2 + \lambda||\nabla\mathbf{X} - \nabla D(\mathbf{P})||_{2,1}\}. \quad (5)$$

Let $\mathbf{Z} = \mathbf{X} - D(\mathbf{P})$ and we can rewrite the problem:

$$\mathbf{Z}^k = \arg\min_{\mathbf{Z}} \{\frac{1}{2}\|\mathbf{Z} - (\mathbf{Y} - D(\mathbf{P}))\|_F^2 + \lambda||\nabla\mathbf{Z}||_{2,1}\}. \quad (6)$$

This alternative problem is therefore a VTV denoising problem [5, 12, 7] and $\mathbf{X}^k$ can be updated by $\mathbf{Z}^k + D(\mathbf{P})$. The slow version of the VTV denoising algorithm [5] is accelerated based on FISTA framework to solve (6), which is summarized in [12, 7]. The fast convergence rate $\mathcal{O}(1/k^2)$ is theoretically guaranteed by FISTA [19, 4].

Algorithm 1 DGS-Fusion

Input: L, λ, $t^1 = 1$, $\mathbf{Y}^0$
for $k = 1$ **to** $Maxiteration$ **do**
  $\mathbf{Y} = \mathbf{Y}^k - \psi^T(\psi\mathbf{X} - \mathbf{M})/L$
  $\mathbf{X}^k = \arg\min_{\mathbf{X}}\{\frac{L}{2}\|\mathbf{X}-\mathbf{Y}\|_F^2 + \lambda||\nabla\mathbf{X} - \nabla D(\mathbf{P})||_{2,1}\}$
  $t^{k+1} = [1 + \sqrt{1 + 4(t^k)^2}]/2$
  $\mathbf{Y}^{k+1} = \mathbf{X}^k + \frac{t^k - 1}{t^{k+1}}(\mathbf{X}^k - \mathbf{X}^{k-1})$
end for

3. Experiment

The proposed method is validated on datasets from Quickbird, Geoeye, SPOT and IKONOS satellites. The resolution of Pan images ranges from 0.41 m to 1.5 m. All the corresponding MS images have lower resolutions with $c = 4$ and contain blue, green, red and near-infrared bands. For convenience, only the RGB bands are presented. Due to the lack of multi-resolution images of the same scene, low resolution images are downsampled from the ground-truth. This strategy is common for comparing fusion algorithms (e.g. [21][22][3][18][9]).

We compare our method with classical methods PCA [6], IHS [11], wavelet [25], Brovey [10] and variation methods P+XS [3], AVWP [18]. The effectiveness of our method is validated via extensive experiments with visual and quantitative analysis. Comparison with P+XS [3] and AVWP [18] demonstrates its efficiency. The parameters for each method are tuned individually according to the authors' suggestion and the best set is selected for each method, respectively. All experiments are conducted using Matlab on a desktop with 3.4GHz Intel core i7 3770 CPU.

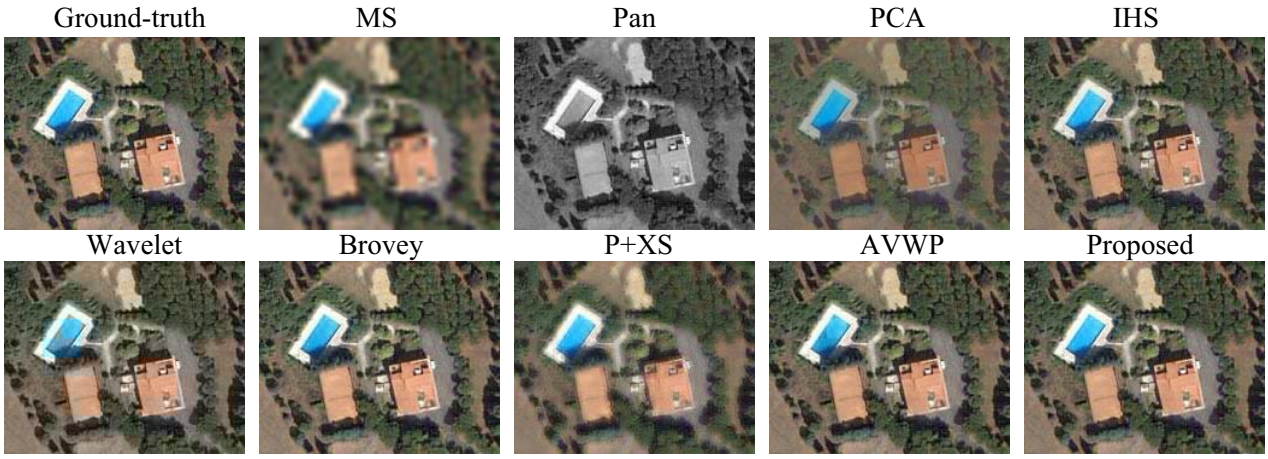

Figure 2. Fusion Results comparison (source: Quickbird). The Pan image has 200×160 pixels. Copyright DigitalGlobe.

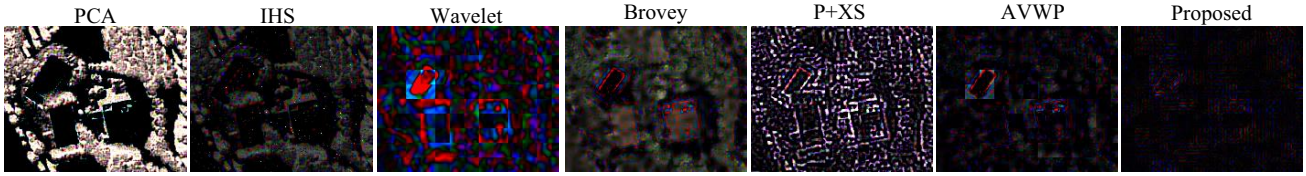

Figure 3. The corresponding error images to those in Figure 2. Brighter pixels represent larger errors.

3.1. Visual Comparison

First, we compare the fusion result by our method with those of previous works [6][11][25][10][3][18]. Figure 2 shows the fusion results as well as the original images captured by the Quickbird satellite. All the methods can produce much better visual images than the original MS image. Obviously, PCA [6] performs the worst. No artifacts can be found on the images produced by IHS [11] and Brovey [10]. However, a closer look shows that the color on these images tends to change, especially on the trees and grass. This is a sign of spectral distortion [20]. Wavelet fusion [25] suffers from both spectral distortion and blocky artifacts (e.g. on the swimming poor). Blurred edges is a general issue in the image fused by P+XS [3]. AVWP [18] performs much better than all of them but it inherits the blocky artifacts of the wavelet fusion.

For better visualization, the error images compared with the ground-truth are presented in Figure 3 at the same scale. From these error images, the spectral distortion, blocky artifacts, and blurriness can be clearly observed. These results are consistent with those presented in previous work [18]. Due to the spectral distortion, the conventional methods are not adapted to vegetation study [20]. Previous variational methods [3][18] try to break such hard assumptions by combining a few weak assumptions. However, such combinations involves more parameters that required to be tuned. Moreover, the fusion from the upsampled MS image often results in inaccuracy. In contrast, we only constrain the spectral information of the fused image to be locally consistent with the original MS image. The fusion results are impressively good from these visual observations.

3.2. Quantitative Analysis

Besides the image used previously, 157 test images of different sizes (from 128×128 to 512×512) are cropped from Quickbird, Geoeye, IKONOS and SPOT datasets, which contain vegetation (e.g. forest, farmland), bodies of water (e.g. river, lake) and urban scenes (e.g. building, road). This test set is much larger than the size of all datasets considered in previous variational methods (31 images in [3], 7 images in [18] and 4 images in [9]). Example images are shown in Figure 4.

To evaluate the fusion quality of different methods, we use four metrics that measure spectral quality and one metric that measures spatial quality. The spectral metrics include the relative dimensionless global error in synthesis (ERGAS) [1], spectral angle mapper (SAM) [1], universal image quality index (Q-average) [23] and relative average spectral error (RASE) [8]. The filtered correlation coefficients (FCC) [25] is used as spatial quality metric. In addition, peak signal-to-noise ratio (PSNR), and root mean squared error (RMSE) and mean structural similarity (MSSIM) [23] are used to evaluate the fusion accuracy when compared with the ground-truth.

The average results and the variance on this test set are

Method	ERGAS	QAVE	RASE	SAM	FCC	PSNR	MSSIM	RMSE
PCA [6]	5.67±1.77	0.664±0.055	22.3±6.8	2.11±1.35	0.972±0.014	20.7±2.7	0.799±0.067	24.1±6.7
IHS [11]	1.68±0.86	0.734±0.011	6.63±3.4	0.79±0.54	0.989±0.006	31.2±4.6	0.960±0.035	8.1±4.2
Wavelet[25]	1.18±0.45	0.598±0.113	4.50±1.6	2.45±1.18	**0.997±0.002**	36.1±3.6	0.983±0.009	4.5±1.9
Brovey [10]	1.22±1.08	0.733±0.011	5.18±4.6	0.61±0.58	0.940±0.170	38.2±5.6	0.989±0.008	9.1±19.7
P+XS[3]	0.89±0.33	0.720±0.036	3.47±1.3	0.66±0.36	0.898±0.024	25.9±3.5	0.854±0.051	14.7±5.4
AVWP[18]	0.46±0.17	0.733±0.013	1.81±0.6	0.69±0.70	0.996±0.002	40.0±3.5	0.991±0.006	2.9±1.0
Proposed	**0.07±0.03**	**0.746±0.004**	**0.3±0.1**	**0.18± 0.11**	**0.997±0.002**	**47.5±3.6**	**0.998±0.001**	**1.1±0.5**
Reference Value	0	1	0	0	1	$+\infty$	1	0

Table 1. Performance Comparison on the 158 remotely sensed images.

Figure 4. Example images used in our experiments. Copyright DigitalGlobe for Quickbird, Geoeye and IKONOS. Copyright CNES for SPOT.

listed in Table 2. The ideal value for each metric is shown in the last row. The results of variational methods [3][18] have much lower values in ERGAS and RASE than those of conventional methods [6][11][25][10]. From QAVE and SAM, the results are comparable to conventional methods. We can conclude that these variational methods can preserve more spectral information. Due to the blurriness, P+XS has the worse spatial resolution in terms of FCC. In terms of error and similarity metrics (PSNR, MSSIM, RMSE), AVWP and P+XS are always the second best and second worst, respectively. Except for the same FCC as the wavelet fusion, our method is consistently better than all previous methods in terms of all metrics. These results are enough to demonstrate the success of our method, where the dynamic gradient sparsity can preserve sharp edges and the spectral constraint keeps accurate spectral information. In terms of PSNR, it can outperform the second best method AVWP by more than 7 dB.

If we consider the prior information that is used, the performance of each algorithm is easy to explain. Conventional projection-substitution methods only treat the input images as vectorial information (i.e. 1D). The difference is the substitution performed on various projection spaces. However, 2D information such as boundaries is not utilized. The boundary information has been considered in both variational methods P+XS [3] and AVWP [18], although their models can not effectively exploit this prior information. Promising results, especially by AVWP, have already achieved over conventional methods. By using the proposed dynamic gradient sparsity, our method has successfully learned more prior knowledge provided by the Pan image. Due to the group sparsity across different bands, our method is less sensitive to noise. These are why our method consistently outperforms the others.

3.3. Efficiency Comparison

To evaluate the efficiency of the proposed method, we compare the proposed method with previous variational methods P+XS [3] and AVWP [18] in terms of both accuracy and computational cost. PSNR is used to measure fusion accuracy. Figure 5 demonstrates the convergence rate comparison of these algorithms corresponding to the images in Figure 2. Inheriting the benefit of the FISTA [4] framework, our method often converges in 100 to 150 outer iterations. AVWP often converges in 200 to 400 iterations. P+XS that uses classic gradient decent method has not converged even with 600 iterations. After each algorithm converged, our method can approximately outperform AVWP by more than 5 dB on this image in terms of PSNR. Note that the later one is the second best method from previous analysis.

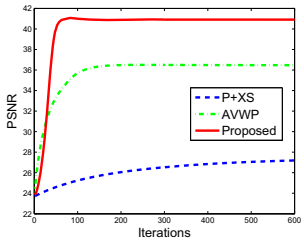

Figure 5. Convergence rate comparison among P+XS, AVWP and the proposed method. The Result corresponds to Figure 2.

The average computational costs of these three methods are listed in Table 3 for different sizes of test images. Both the proposed method and AVWP terminate when a fixed tolerance is reached (e.g. 10^{-3} of the relative change on $\mathbf{X}$). The computational cost of our method tend to be linear from these results. Even the second fastest method AVWP

takes about 50% more time than ours on an image of 512 by 512 pixels. These comparisons are sufficient to demonstrate the efficiency and effectiveness of our method.

	128×128	256×256	384×384	512×512
P+XS	6.7	16.0	48.3	87.4
AVWP	1.7	8.3	28.2	54.7
Proposed	**1.4**	**5.0**	**19.3**	**36.8**

Table 2. Computational time (second) comparison.

3.4. Discussion

The gradient prior information and joint structure have been separately utilized in other image enhancement tasks [16, 17]. Such success further demonstrates the effectiveness of our modeling. The proposed method is not sensitive to an exact downsampling scheme. When the actual downsampling is cubic interpolation, the same result can be obtained if we use either cubic or bilinear interpolation. It is only sightly worse when we use an averaging strategy.

4. Conclusion

We have proposed a novel and powerful variational model for pan-sharpening with local spectral consistency and dynamic gradient sparsity. The model naturally incorporates the gradient prior information from a high resolution Pan image and spectral information from an MS image. Moreover, our model also exploits the band correlations of the fused image itself, which has not yet considered in any previous method. An efficient optimization algorithm has been devised to solve the problem, with very fast convergence speed. Extensive experiments are conducted on 158 images stemming from a variety of sources. Due to the proposed unique techniques, our methods is corroborated to consistently outperforms the state-of-the-arts in terms of both spatial and spectral qualities.

Acknowledgement

We sincerely thank Dr. Darin Brezeale for reading a preliminary version of this work and providing valuable feedback.

References

[1] L. Alparone, L. Wald, J. Chanussot, C. Thomas, P. Gamba, and L. M. Bruce. Comparison of pansharpening algorithms: Outcome of the 2006 grs-s data-fusion contest. *IEEE Trans. Geoscience and Remote Sensing*, 45(10):3012–3021, 2007.

[2] I. Amro, J. Mateos, M. Vega, R. Molina, and A. K. Katsaggelos. A survey of classical methods and new trends in pansharpening of multispectral images. *EURASIP Journal on Advances in Signal Processing*, 2011(79):1–22, 2011.

[3] C. Ballester, V. Caselles, L. Igual, J. Verdera, and B. Rougé. A variational model for P+XS image fusion. *IJCV*, 69(1):43–58, 2006.

[4] A. Beck and M. Teboulle. A fast iterative shrinkage-thresholding algorithm for linear inverse problems. *SIAM J. Imaging Sciences*, 2(1):183–202, 2009.

[5] X. Bresson and T. F. Chan. Fast dual minimization of the vectorial total variation norm and applications to color image processing. *Inverse problems and imaging*, 2(4):455–484, 2008.

[6] P. S. Chavez, Jr, S. C. Sides, and J. A. Anderson. Comparison of three different methods to merge multiresolution and multispectral data: Landsat tm and spot panchromatic. *Photogrammetric Engineering and Remote Sensing*, 57(3):295–303, 1991.

[7] C. Chen, Y. Li, and J. Huang. Calibrationless Parallel MRI with Joint Total Variation Regularization. In *Proc. Medical Image Computing and Computer-Assisted Intervention (MICCAI)*, pages 106–114, 2013.

[8] M. Choi. A new intensity-hue-saturation fusion approach to image fusion with a tradeoff parameter. *IEEE Trans. Geoscience and Remote Sensing*, 44(6):1672–1682, 2006.

[9] F. Fang, F. Li, C. Shen, and G. Zhang. A variational approach for pan-sharpening. *IEEE Trans. Image Processing*, 22(7):2822–2834, 2013.

[10] A. R. Gillespie, A. B. Kahle, and R. E. Walker. Color enhancement of highly correlated images. i. decorrelation and hsi contrast stretches. *Remote Sensing of Environment*, 20(3):209–235, 1986.

[11] R. Haydn, G. W. Dalke, J. Henkel, and J. E. Bare. Application of the IHS color transform to the processing of multisensor data and image enhancement. In *Proc. International Symposium on Remote Sensing of Environment*, 1982.

[12] J. Huang, C. Chen, and L. Axel. Fast Multi-contrast MRI Reconstruction. In *Proc. Medical Image Computing and Computer-Assisted Intervention (MICCAI)*, pages 281–288, 2012.

[13] J. Huang, X. Huang, and D. Metaxas. Learning with dynamic group sparsity. In *Proc. ICCV*, pages 64–71, 2009.

[14] J. Huang, S. Zhang, H. Li, and D. Metaxas. Composite splitting algorithms for convex optimization. *Comput. Vis. Image Und.*, 115(12):1610–1622, 2011.

[15] J. Huang, T. Zhang, and D. Metaxas. Learning with structured sparsity. *J. Mach. Learn. Res.*, 12:3371–3412, 2011.

[16] D. Krishnan and R. Fergus. Dark flash photography. In *Proc. SIGGRAPH*, 2009.

[17] M.-Y. Liu, O. Tuzel, and Y. Taguchi. Joint geodesic upsampling of depth images. In *Proc. CVPR*, pages 169–176, 2013.

[18] M. Möller, T. Wittman, A. L. Bertozzi, and M. Burger. A variational approach for sharpening high dimensional images. *SIAM J. Imaging Sciences*, 5(1):150–178, 2012.

[19] M. W. Schmidt, N. Le Roux, F. Bach, et al. Convergence rates of inexact proximal-gradient methods for convex optimization. In *Proc. NIPS*, pages 1458–1466, 2011.

[20] C. Thomas, T. Ranchin, L. Wald, and J. Chanussot. Synthesis of multispectral images to high spatial resolution: A critical review of fusion methods based on remote sensing physics. *IEEE Trans. Geoscience and Remote Sensing*, 46(5):1301–1312, 2008.

[21] V. Vijayaraj, C. G. O'Hara, and N. H. Younan. Quality analysis of pansharpened images. In *Proc. International Geoscience and Remote Sensing Symposium*, 2004.

[22] L. Wald, T. Ranchin, and M. Mangolini. Fusion of satellite images of different spatial resolutions: assessing the quality of resulting images. *Photogrammetric Engineering and Remote Sensing*, 63(6):691–699, 1997.

[23] Z. Wang and A. C. Bovik. Modern image quality assessment. *Synthesis Lectures on Image, Video, and Multimedia Processing*, 2(1):1–156, 2006.

[24] M. Yuan and Y. Lin. Model selection and estimation in regression with grouped variables. *J. the Royal Statistical Society: Series B (Statistical Methodology)*, 68(1):49–67, 2005.

[25] J. Zhou, D. L. Civco, and J. A. Silander. A wavelet transform method to merge landsat tm and spot panchromatic data. *International J. Remote Sensing*, 19(4):743–757, 1998.